

Geophysical Research Letters



RESEARCH LETTER

10.1029/2020GL092234

Key Points:

- Presently, 183 submarine canyons are connected to the shoreline (within 6 km) along the world's major continents
- Narrow shelves and high shelf gradients precondition the maintenance of canyon-head connectivity to the shore
- Canyon heads preferentially remain connected to the shore offshore river catchments with resistant bedrock and high water discharge

Supporting Information:

Supporting Information may be found in the online version of this article.

Correspondence to:

A. Bernhardt,
anne.bernhardt@fu-berlin.de



Citation:

Bernhardt, A., & Schwanghart, W. (2021). Where and why do submarine canyons remain connected to the shore during sea-level rise? Insights from global topographic analysis and Bayesian regression. *Geophysical Research Letters*, 48, e2020GL092234. <https://doi.org/10.1029/2020GL092234>

Received 23 DEC 2020

Accepted 19 APR 2021

Where and Why Do Submarine Canyons Remain Connected to the Shore During Sea-Level Rise? Insights From Global Topographic Analysis and Bayesian Regression

Anne Bernhardt¹  and Wolfgang Schwanghart² 

¹Institute of Geological Sciences, Freie Universität Berlin, Berlin, Germany, ²Institute of Environmental Sciences and Geography, Potsdam University, Potsdam-Golm, Germany

Abstract The efficiency of sediment routing from land to the ocean depends on the position of submarine canyon heads with regard to terrestrial sediment sources. We aim to identify the main controls on whether a submarine canyon head remains connected to terrestrial sediment input during Holocene sea-level rise. Globally, we identified 798 canyon heads that are currently located at the 120m-depth contour (the Last Glacial Maximum shoreline) and 183 canyon heads that are connected to the shore (within a distance of 6 km) during the present-day highstand. Regional hotspots of shore-connected canyons are the Mediterranean active margin and the Pacific coast of Central and South America. We used 34 terrestrial and marine predictor variables to predict shore-connected canyon occurrence using Bayesian regression. Our analysis shows that steep and narrow shelves facilitate canyon-head connectivity to the shore. Moreover, shore-connected canyons occur preferentially along active margins characterized by resistant bedrock and high river-water discharge.

Plain Language Summary Since the last glaciation about 20,000 years ago, sea level has risen by about 120 m. As a consequence, most coastlines have migrated landward, inundating large shelf areas. Some of these areas are now dissected by submarine canyons. However, with only 4% of the world's submarine canyons reaching today's coastline, these canyons remain the exception. Here, we aim to identify the environmental factors and processes that control whether rates of headward canyon incision can keep pace with landward migration of the coastline during the Holocene. We determine 34 variables that potentially predict whether a canyon remains connected to the coastline. We find that shore-connected canyons preferentially occur along continental margins with narrow and steep shelves, such as the Mediterranean active margin and the Pacific coast of Central and South America. Moreover, our analysis supports the occurrence of such canyons offshore river basins, that are characterized by resistant bedrock and high water discharge. Such rivers deliver coarse-grained sediment to submarine canyons, which can erode the canyon head and floor. To this end, our analysis offers new insights into the formation and maintenance of submarine canyons that are required to efficiently transport sediments, pollutants, and organic carbon from rivers to the ocean floor.

1. Introduction

Submarine canyons are prime conduits for sediment-laden flows that link terrestrial sediment sources with deep-marine depocenters. The efficiency at which canyons route sediments is at least partly controlled by how far they extend into the shelf. If the distance between the canyon head and the shore is short, terrestrial sediment, associated pollutants, and organic carbon can be efficiently delivered to the deep ocean (Azaroff et al., 2020; Covault et al., 2007; Dominguez-Carrió et al., 2020; Galy et al., 2007; Kane & Clare, 2019). We refer to such canyons as shore-connected canyons hereafter.

Whether and where shore-connected canyons occur relates to the canyons' ability to erode headward at a pace that keeps up with millennial-scale sea-level rise (e.g., after the Last Glacial Maximum [LGM]) (Maufrey et al., 2017). It is remarkable that ~30% of submarine canyons are incised into the shelf but only few canyons are connected to the present-day shoreline (Harris & Whiteway, 2011). However, the detailed controls on why a submarine canyon is incised into the shelf or why it remained connected to terrestrial sediment

© 2021. The Authors.

This is an open access article under the terms of the [Creative Commons Attribution License](https://creativecommons.org/licenses/by/4.0/), which permits use, distribution and reproduction in any medium, provided the original work is properly cited.

supply during rising sea level are poorly understood (Harris & Whiteway, 2011; Smith et al., 2017, 2018). Several, possibly related, factors (Shepard, 1981) were proposed to control canyon occurrence and shelf incision, including narrow continental shelves along active margins (Normark et al., 2009), seismic activity (Mountjoy et al., 2018), high shelf gradient (Sweet & Blum, 2016), high sediment flux from onshore catchments (Harris & Whiteway, 2011; Pratson et al., 2007), mass wasting along steep continental slopes (Pratson & Coakley, 1996; Pratson et al., 1994), and submarine groundwater seepage (Pratson et al., 2007).

Based on a global compilation of submarine canyons, Harris and Whiteway (2011) showed that shelf-incising canyons prevail along the western, tectonically active margins of the Americas that are characterized by high sediment supply. Smith et al. (2017) focused on the West Coast of the United States and found no correlation between canyon occurrence and shelf gradient. Instead, their analysis showed that coarse sediment from onshore catchments exposing durable bedrock governs offshore canyon-head incision, modulated by wave focusing of canyon bathymetry (Smith et al., 2017, 2018). Yet, whether onshore processes and lithological composition control headward submarine canyon erosion at the global scale has not been investigated.

We study global patterns of shore-connected canyons to identify the main controls on their occurrence. Our analysis is driven by two hypotheses: First, we hypothesize that submarine canyon heads remain connected to the shore upon postglacial sea-level rise if the shelf is narrow and steep. Second, we test the hypothesis of Smith et al. (2017, 2018) that submarine canyon heads remain connected to the shoreline when located offshore tectonically uplifting regions with durable bedrock. We categorize canyon heads as “shore-connected” and as “close to the 120m-depth contour” and assert that the latter may have been connected to the shore during the LGM but were unable to erode headwards to the present-day shoreline. We then predict shore-connected canyons using Bayesian penalized regression, a technique that selects predictor variables that are relevant for predicting a specific response variable.

2. Methods and Data

Our study relies on the Shuttle-Radar-Topography Mission (SRTM30_PLUS) 30-arc-second database (~1 km resolution at the equator) (Becker et al., 2009). We excluded islands and oceanic plateaus and limited our analysis to 50°N and 50°S where predictor variables (Table 1) are available.

2.1. Submarine Canyon Variables

We used the data set from Harris et al. (2014) who mapped “large” canyons that extend over a depth range of at least 1,000 m and are incised at least 100 m. Hence, this analysis focuses on large features and omits smaller canyons. We manually mapped canyon heads, assigned them to the submarine-canyon polygon of Harris et al. (2014) (Figure 1), and computed the shortest Euclidean distance from each canyon head to the present-day shoreline and to the 120m-depth contour (LGM shoreline). Canyon heads located <6 km away from either shoreline were classified as “shore-connected present” or as “120m-contour canyons”, respectively (Figures 1a and 1b). The distance exceeds the offshore limit of longshore sediment transport (up to 5 km; Sweet & Blum, 2016) by 1 km to account for uncertainties in mapping due to the latitudinally variable spatial resolution of the SRTM30_PLUS data set. We assume that “shore-connected canyons” receive terrigenous sediment directly from the shore through either longshore sediment transport or by direct river input. With this approach, we potentially include canyons that are not strictly connected to the ocean littoral cell but should capture all truly connected “large” canyons. We manually corrected canyon-head misclassifications during visual inspection. Although some canyons (Swatch-of-No-Ground, located 150 km off coast, Rogers et al., 2015; Indus canyon, 17 km, Li et al., 2018) presently receive terrestrial sediment through cliff-form progradation, we did not classify these as shore-connected.

2.2. Terrestrial Variables

Topographic analysis was conducted with ArcGIS, MATLAB, and TopoToolbox (Schwanghart and Scherler, 2014). Terrestrial drainage-basin metrics (elevation, gradient, area, river steepness (ksn)), and river outlets were determined using the 500-m-grid and flow directions of the HydroSHEDS compilation (Lehner et al., 2008) (Table 1).

Table 1
Summary of Predictor Variables

Predictor variable	Unit	Description and computation	Data source	Abbreviation in table	Reason for inclusion
Terrestrial predictors					
are weighted using Equation 1:					
$\lambda_i = \frac{A_i}{d_i^3} / \left(\sum_i \frac{A_i}{d_i^3} \right)$					
Distance to the nearest river outlet	km	Euclidian distance to the nearest river outlet	SRTM30_PLUS (Becker et al., 2009) HydroSHEDS (Lehner et al., 2008)	d_weighted	Short d_weighted increases fluvial sediment supply to canyon heads
Max. & mean elevation, area, gradient of onshore catchment (present day)	m, km ² , m/m	upslopestats and gradient function of TopoToolbox (MATLAB)	See above	elev_max_weighted, elev_mean_weighted, area_weighted, grad_weighted	Characterization of river catchments adjacent to canyon
Mean river steepness index in onshore catchment (present day)	dimensionless	ksn and upstreammean function of TopoToolbox	See above	ksn_weighted	Characterization of river profiles adjacent to canyon
Mean annual discharge of onshore catchment Qw, Qw_weighted/area_weighted	m ³ /s, m ³ /s/km ²	flowacc function of TopoToolbox	Fekete et al. (2002)	Qw_weighted, Qw_area	High Qw may foster high sediment supply to the canyon head
Modeled suspended sediment flux (pre-human) Qs, sediment yield Qsy (Qs_weighted/area_weighted)	kg/s, kg/s/km ²	Qs at river outlets was assigned to the HydroSHEDS stream network using the knnsearchlatlon & matchpairs function of TopoToolbox/MATLAB	Qs values of Syvitski and Kettner (2011) (BQART)	Qs_weighted, Qsy	High Qs may foster canyon-head erosion
Bedload estimated from empirical equation of Bagnold & Métivier (pre-human)	kg/s	$Q_{bed} = 0.8 \times Q_s^{0.5926}$ $Q_{bed} = aQ_s^b \text{ for } Q_s \leq \left(\frac{a}{c} \right)^{1/(d-b)}$ $Q_{bed} = cQ_s^d$ a = 0.833 ^ (1 - b); b = 1.3240; c = 0.437 ^ (1 - d); d = 0.647;	Bagnold (1966), Syvitski and Saito (2007), Métivier et al. (2004), Meunier et al. (2006); Qs values of Syvitski and Kettner (2011)	QbBagnold_weighted, QbMétivier_weighted	High Qb may foster canyon-head erosion
Peak ground acceleration	m/s ²	Peak ground acceleration from the Global Seismic Hazard Map of the Global Seismic Hazard Assessment Program (GSHAP) - which depicts PGA with a 10% probability of exceedance in 50 years- was assigned to each river outlet using the flowacc function of TopoToolbox	Shedlock et al. (2000)	GSHAP_weighted	Proxy for tectonic activity, intense seismic shaking may trigger erosive turbidity currents

Table 1
Continued

Predictor variable	Unit	Description and computation	Data source	Abbreviation in table	Reason for inclusion
Weighted global erodibility index (GEroID)	dimensionless	GEroID ranges from 1.0 (low erodibility) to 3.2 (high erodibility), area-weighted mean of GEroID for each drainage basin was assigned to each river outlet using the <i>upslopestats</i> function of TopoToolbox	Global erodibility index data set (GEroID) of Moosdorf et al. (2018)	ero_index_weighted	Sediment supply from low-erodibility bedrock may enhance canyon-head erosion
Mean annual rainfall	mm/day	Area-weighted mean of annual rainfall for each drainage basin was assigned to each river outlet using the <i>upslopestats</i> function of TopoToolbox	Courtesy of B. Bookhagen	TRMM_mean_weighted	High precipitation may cause high erosion & high sediment supply to the canyon head
Yearly standard deviation (STDV) of the daily rainfall	mm/day	Area-weighted mean of the STDV of the mean annual rainfall for each drainage basin was assigned to each river outlet using the <i>upslopestats</i> function of TopoToolbox	Courtesy of B. Bookhagen	TRMM_STDV_weighted	Unevenly distributed rainfall may cause high instantaneous sediment discharge (see below)
The ratio of the 90th to 50th percentile of the mean annual rainfall	dimensionless	This ratio is a measure for how extreme rainfall is, high values indicate extreme rainfall events, area-weighted mean of the 90th/50th percentile of the mean annual rainfall for each catchment was assigned to each river outlet using the <i>upslopestats</i> function of TopoToolbox	Boers et al. (2014)	TRMM_90_50_weighted	Extreme rainfall events may result in high instantaneous sediment supply and possibly in hyperpycnal flows flowing into canyon heads
Marine predictors	<i>All marine predictors are not weighted</i>				
Gradient of the adjacent shelf	degree	Computed outline of shelf shape file (Harris et al., 2014), Laplace interpolation between shelf boundaries to create a smoothed shelf without submarine canyons, computed mean gradient of the smoothed shelf surrounding each canyon head in a circular shaped polygon with a radius of 10 km	SRTM30_PLUS Becker et al. (2009) & Harris et al. (2014)	shelf_gradient	High shelf gradient can promote erosive turbidity currents that foster canyon-head incision

Table 1
Continued

Predictor variable	Unit	Description and computation	Data source	Abbreviation in table	Reason for inclusion
Gradient of the adjacent continental slope	degree	Analogous to shelf_gradient but using a circular shaped polygon with a radius of 80 km	See above	csgradient	High gradient can promote erosive turbidity currents
Max. & mean shelf width (present day)	km	Determined the 100 nearest-neighbor DEM pixels (86 km) along the outer shelf boundary from each canyon head (using <i>bwdist</i> & <i>knnsearch</i> in MATLAB) & calculated the mean shelf width from these; where shelf-incising canyons reduced shelf width, results were corrected after visual inspection	Harris et al. (2014)	dshelf_mean, dshelf_max	Narrow shelves have been suggested to facilitate canyon-to-shore connection
Max. & mean shelf width (LGM)	km	identical calculation to the present-day shelf width, but based on SRTM30_PLUS DEM, where 120 m were added to the elevation data	See above	dshelf_mean_LGM, dshelf_max_LGM	Narrow shelves may facilitate canyon-to-shore connection
Difference between LGM and present-day shelf width	km	dshelf_mean minus dshelf_mean_LGM, the distance a canyon head has to erode backwards to remain connected to the shore during Holocene sea-level rise	See above	dshelf_diff	We hypothesize that short dshelf_diff facilitates canyon-to-shore connection
Max. & mean depth of the shelf edge	m	Water depth of shelf edge was calculated using mapped shelf outline and SRTM_30plus data, shelf edge depth was assigned to each canyon head using from the 20 nearest neighbor DEM pixels (17 km) using the the <i>knnsearch</i> function in a 20 cell window	SRTM30_PLUS Becker et al. (2009) & Harris et al. (2014)	max shelf_edge_z, mean shelf_edge_z	A deep location of the shelf edge may lead to more erosive turbidity currents at the shelf-slope transition
Max. & mean storm surge height	m	Determined the 20 nearest-neighbor DEM pixels from the GTSR data set along the coast from each submarine canyon head (using the <i>knnsearch</i> function in MATLAB) and calculated the mean & max. storm surge heights from these 20 pixels	Global Tide and Surge Reanalysis (GTSR) Muis et al. (2016)	mean_storm_surge, max_storm_surge	Quantifies storm surges & extreme sea levels, which may contribute to canyon-head erosion

Table 1
Continued

Predictor variable	Unit	Description and computation	Data source	Abbreviation in table	Reason for inclusion
Wave height & wave period	m	Wave height & period from Sentinel 2 data	Bergsma and Almar (2020)	wave_height_m, wave_period_m	Wave action has been postulated to foster canyon-head incision
Depth of closure	m	Depth of closure along the adjacent coastline, quantifies the max. water depth of the ocean littoral cell	Bergsma and Almar (2020)	depth_of_closure_m	The littoral cell can serve as a major sediment contributor to canyon heads
<p>Submarine groundwater discharge predictors are weighted using Equation 2: $\lambda_j = \frac{1}{d_j^3} / \left(\sum_i \frac{1}{d_i^3} \right)$</p> <p>All modeled submarine groundwater discharge (SGD) parameters from Luijendijk et al. (2020):</p> <p>To assign a weighted submarine groundwater discharge value SGD, we chose the centroid of each coastal watershed polygon provided by the authors and performed the weighting to the nearest point on the coast with regard to the canyon head</p>					
Modeled fresh SGD	m ² /yr		Luijendijk et al. (2020)	fsgd_best_weighted	Submarine groundwater seepage may foster canyon-head incision
Modeled near-shore terrestrial discharge (NGD)	m ² /yr		Luijendijk et al. (2020)	ngd_best_weighted	See above
Modeled total coastal groundwater discharge (CGD)	m ² /yr	CGD = NGD + SGD	Luijendijk et al. (2020)	cgd_best_weighted	See above

We obtained estimates of water discharge (Qw) at each river outlet by integrating annual runoff from the Global Runoff Data Centre (Fekete et al., 2002). We used the BQART model for pre-human riverine suspended sediment flux (Qs) (Syvitski & Kettner, 2011), which plays an important role in offshore sediment transport (Hage et al., 2019). Bedload was estimated by two empirical equations (Table 1). We extracted a mean, area-weighted erodibility index for each catchment using the global erodibility index (GEroID) of Moosdorf et al. (2018), ranging from low-erodibility metamorphic rocks (=0.8) to high erodibility (=3.2) for unconsolidated sediments. Area-weighted means of annual rainfall and its variability were calculated using Tropical-Rainfall-Measurement-Mission data (TRMM, courtesy of Boers et al. [2014]). Finally, we assigned peak-ground accelerations (PGAs) to river outlets using the Global Seismic Hazard Map (Shedlock et al., 2003).

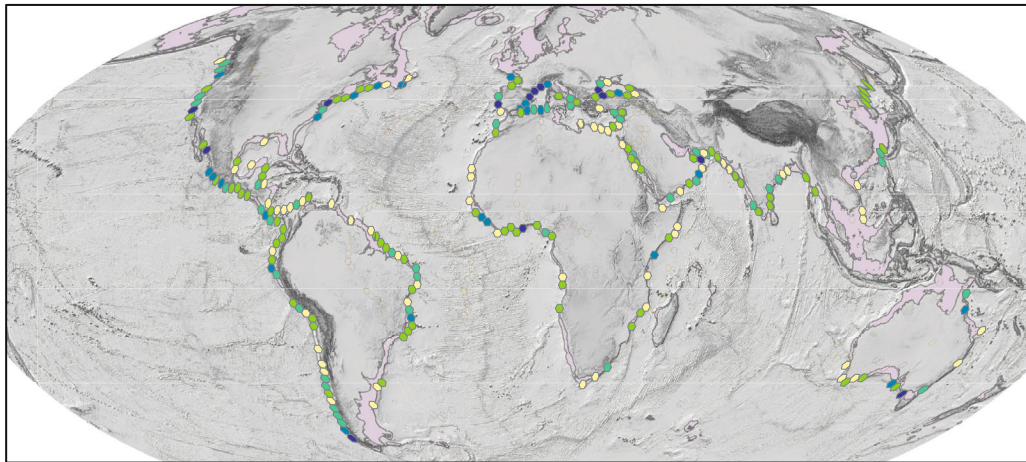
2.2.1. Weighting of Terrestrial Variables to Submarine Canyon Heads

To assign terrestrial variables to submarine canyons, we first determined the closest point on the shoreline (XY_{coast}) for each canyon head (Figure 1c), and then computed the distance between XY_{coast} and river outlets on the adjacent continent. These distances d_i together with the catchment areas A_i of each river outlet i served as weights in a distance-weighted averaging approach. Specifically, we calculated the weights λ_i as:

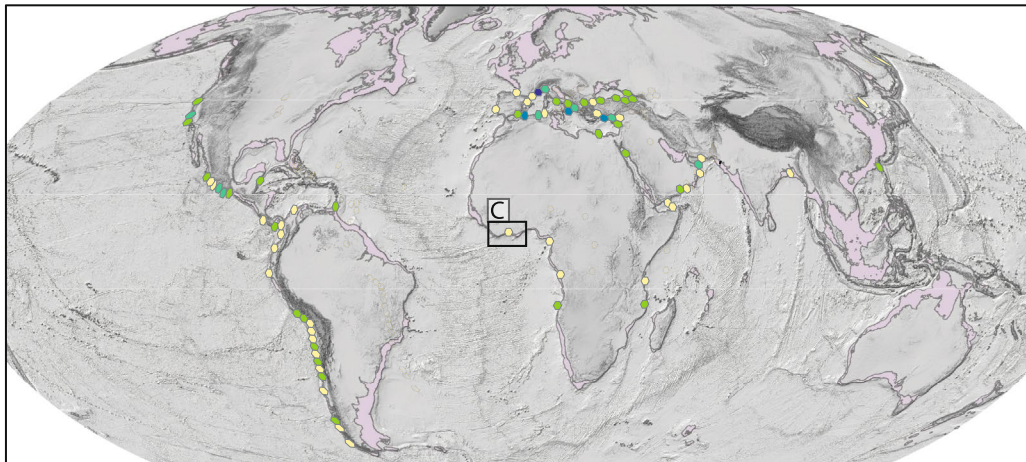
$$\lambda_i = \frac{A_i}{d_i^3} / \left(\sum_i \frac{A_i}{d_i^3} \right), \quad (1)$$

and assigned the weighted average to the corresponding canyon head. Our weighting scheme reflects that a one-to-one assignment of river outlets to canyon heads is often ambiguous and accounts for the increased importance of nearby and large catchment outlets (Figure S3). Moreover, our approach exonerates us from choosing an arbitrary number of drainage basins that may shed sediment into a particular submarine

A Number of submarine canyon heads close to the 120m-depth contour (shoreline at the Last Glacial Maximum)



B Number of shore-connected submarine canyon heads at present



Number of canyon-head type per hexagon (size: 50,000 km²)

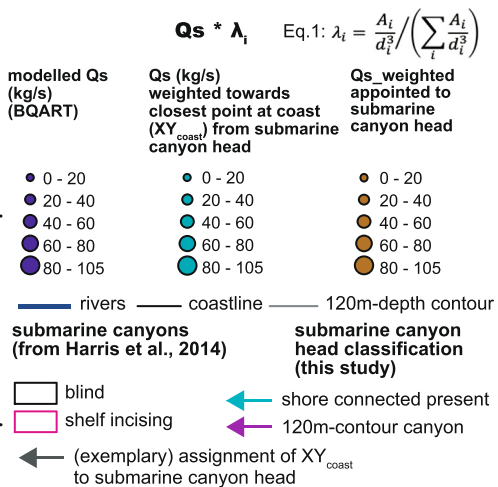
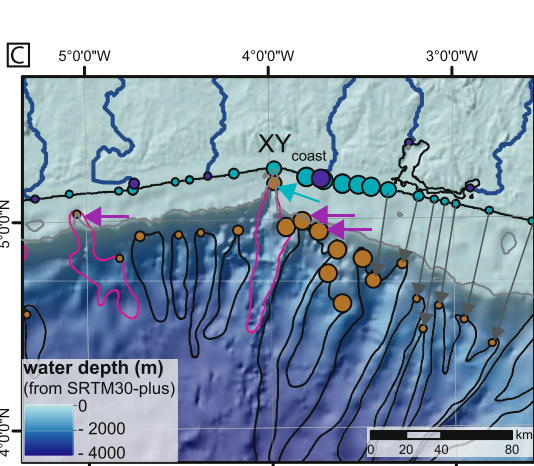
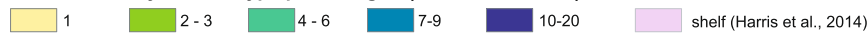


Figure 1. (a) Global canyon-head numbers close to the 120m-depth contour per hexagon (50,000 km²) and (b) of shore-connected canyons. (c) Illustration of the weighting calculation using suspended sediment load (Qs; Syvitski & Kettner, 2011) offshore the Ivory Coast. Most canyons are “blind” and two canyons are shelf-incising. Note that one canyon can have several canyon heads. Three canyon heads are classified as “120m-contour canyons” and only the head of the “Trou-sans-Fond” canyon presently connects to the shore.

canyon. We weighted the variables toward XY_{coast} and not to the canyon head itself to avoid incorporating the canyon-head-to-shore distance into the predictor variables, as this is implicitly what we are aiming to predict.

2.3. Submarine Groundwater Discharge

Luijendijk et al. (2020) globally simulated coastal fresh submarine groundwater discharge (SGD). To assign weighted SGDs to canyon heads, we computed the centroid of each coastal watershed, assigned the SGD to that centroid, and weighted the value by its distance (d) to each XY_{coast} of each canyon head using the weighting factor λ :

$$\lambda_j = \frac{1}{d_j^3} / \left(\sum_i \frac{1}{d_i^3} \right) \quad (2)$$

2.4. Marine Variables

To acquire the mean gradient of the continental slope in the vicinity of canyon heads, we extracted the outlines of the slope shapefile of Harris et al. (2014). We set elevation values within the extent of canyons to NoData and used a Laplacian interpolation to smoothly interpolate inward from these outlines. The technique is referred to as image inpainting (Stolle et al., 2019) and reconstructs a continental slope devoid of canyons. Analogously, we calculated the shelf gradient adjacent to each canyon head using the shelf shapefile of Harris et al. (2014). To calculate shelf width at each canyon head, we extracted pixels at the oceanward shelf boundary and calculated the shortest Euclidian distance to the shoreline. We chose the 100 nearest-neighbor pixels (~86 km) along the oceanward boundary and calculated the mean shelf width from these pixels. We used a large number of nearest-neighbors to minimize the impact of canyon-head indentation into the shelf (Figure 1c). Results were inspected visually and corrected where wide canyons decreased shelf width. For the LGM shelf width, the same calculation was based on a digital elevation model (DEM) where 120 m of elevation were added to each pixel to simulate the LGM landscape. Shelf-edge depth was calculated by extracting the water depth from the 20 nearest-neighbor pixels (~17 km) of the outer shelf boundary. We assigned storm-surge heights of 1-in-100 years extreme sea levels of Muis et al. (2016) to each canyon head. Bergsma and Almar (2020) extracted global wave heights and periods from ESA's Sentinel2 constellation and calculated the depth of closure (maximum water depth of littoral sediment transport; Hallermeier, 1980). We extracted wave height, period, and depths of closure for each XY_{coast} and assigned these to adjacent canyon heads.

2.5. Predictive Modeling—Bayesian Penalized Regression

This study aims to identify the controls on continued shelf incision and maintenance of canyon-head-to-shore connectivity. We computed a hexagonal net (50,000 km²/hexagon) and assigned the number of shore-connected canyon heads in each hexagon (Figure 1b). This is the number we predict (the “response”), using 34 predictor variables (“predictors,” Table 1). To extract the weighted predictors for each hexagon, we computed the hexagon midpoints and their corresponding nearest location at the coast ($XY_{\text{coast-hexgrid}}$) and weighted the predictors for individual canyon heads onto this coastal location (Equations 1 and 2).

To identify the most important predictors and to globally predict shore-connected canyon heads, we employed Bayesian penalized regression. Bayesian statistics apply probabilities to statistical problems offering a way to learn from new data to update prior beliefs while accounting for uncertainties (Efron, 2013; Korup, 2021). A frequentist approach to penalization is Lasso regression which uses a penalty term to shrink small regression coefficients to zero (hence reducing or eliminating unimportant predictors) (Tibshirani, 2011). In Bayesian penalized regression, penalization is incorporated through the choice of prior distribution (e.g., van Erp et al., 2019). We used *bayesreg*, a MATLAB toolbox for fitting Bayesian penalized regression models (Makalic & Schmidt, 2016). All predictors were centered and scaled. As we predict counts of shore-connected canyons per hexagon, we chose a Poisson distribution for the response (see Supporting Information [SI]). Our choice of shrinkage prior followed the procedure of van Erp (2020) (SI includes

prior-sensitivity analyses, Figures S4–S7). Finally, we quantified the importance of each predictor adopting the Bayesian feature-ranking algorithm of Makalic and Schmidt (2011). The rank corresponds to the strength of the association between the predictor and the response (Tables S1–S5) and is based on the 75th percentile of the complete set of rankings for each posterior sample (SI includes a complete list of model parameters).

3. Results

3.1. Shore-Connected Canyon Occurrence

Our data set comprises 4,633 canyon heads, of which 2,765 are classified as blind canyons and 1,702 as shelf-incising. From the latter, 798 were classified as 120 m-contour canyons and 183 as shore-connected canyons. 120m-contour canyons occur globally along passive and active margins (Figure 1a). In contrast, during today's sea-level highstand, most shore-connected canyons straddle along active margins ($n = 114$, Figure 2a) with spatial hotspots along the Mediterranean active margin, and the Pacific coast of central South America and Central America (Figure 1b). Moreover, shore-connected canyons occur frequently along the Californian coast, the Indian-Ocean coast of the Arabic Peninsula and the Eastern Black Sea. Isolated shore-connected canyons occur along the coasts of Africa (Figure 1b).

Figure 2b shows the number of shore-connected canyons per hexagon plotted against the four highest-rank predictors (Figure 3d). 120m-contour canyons occur at shelf widths from <2 to 400 km (Figure S2), whereas shore-connected canyons occupy narrow shelf widths from <2 to 31 km (Figure 2b). Only 8 shore-connected canyons occur at shelf widths between 20 and 31 km, 33 at shelf widths between 10 and 20 km, and the majority occurs at shelves <10 km wide. Shore-connected canyons occur preferentially where shelf gradients exceed 0.5° , the difference between the present-day and LGM shelf width is minimal (<27 km), and become most abundant at differences <9 km. One exception is the Congo canyon which occurs at a ~ 50 -km-wide shelf (Figure S2). Shore-connected canyons occur along a wide range of erodibility indices but are absent at highly erodible catchment lithologies ($GEroID > 2$). The maximum number of shore-connected canyons ($n = 20$) is located offshore southern France.

3.2. Prediction of Shore-Connected Canyons

Our penalized regression models with different prior distributions predict the number of canyon heads in the hexagon tiles reasonably well with average prediction errors of $RMSE = 1.2$ and an explained variance of $\sim 50\%$ (pseudo- R^2 of 0.5). Model performance, model parameters, and their posterior distributions remain largely unaffected by the choice of prior distribution (Figures S5 and S6). Among the prior distributions, sampling with a lasso-shrinkage prior was most effective and thus we show the results of this model hereafter.

Predictions of our model are largely consistent with regional hotspots of shore-connected canyons along the Pacific coast of central South America and Central America, and the Mediterranean active margin (Figures 3a and 3b). Shore-connected canyons along the eastern Black Sea and some along the Indian-Ocean coast of the Arabic Peninsula are also identified. However, the model underestimates the frequency of shore-connected canyons along the Californian coast and the African passive margins (Figure 3). While the spatial patterns of modelled and actual shore-connected canyons are consistent, model residuals indicate high uncertainties in predicting spatial densities of canyons (Figure 3c).

Figure 3d shows the posterior distributions of the regression coefficients of the 10 top-ranked predictors (Table S1). Variable ranking reveals the shelf gradient and the erodibility index as the top two predictors and the only predictors whose posterior distributions do not include zero in their 95% credible interval (regression coefficients of zero indicate no predictive value) (Figure 3d and Table S1). Two climatic parameters (Q_w and TRMM 90/50 percentile) are ranked fifth and seventh and river bedload ($Q_{bBagnold}$) ranks tenth.

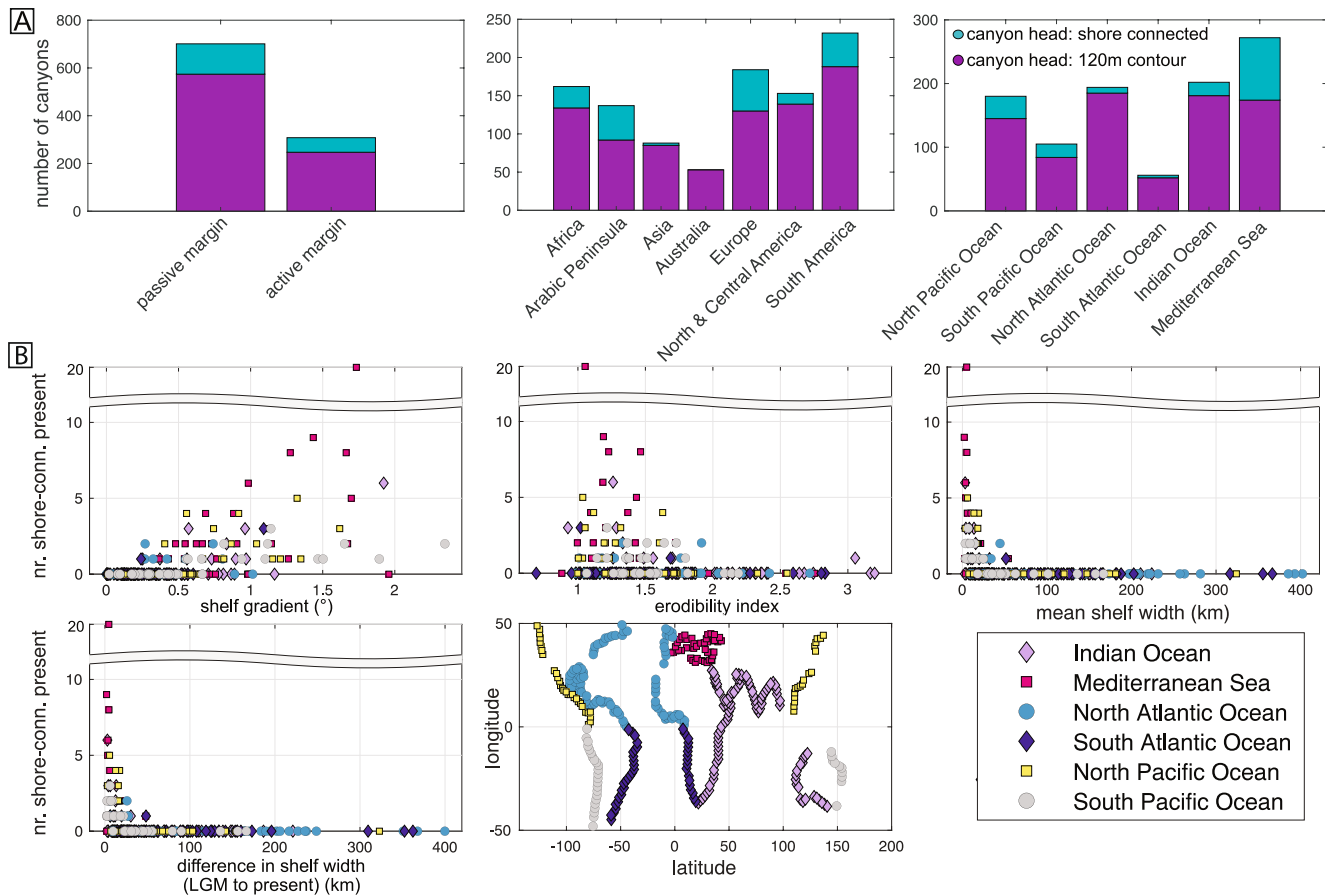


Figure 2. (a) Distribution of canyon-head types along margin types, continents, and oceans. (b) The four most important predictors plotted against the number of shore-connected canyon heads per hexagon. Data points with fraction = 0 represent hexagons that contain 120m-contour canyon heads, but no shore-connected canyons.

4. Discussion

4.1. Data Limitations

Based on Bayesian reasoning and guarded against overfitting by applying penalized regression, we have identified credible predictors for shore-connected canyon occurrence along the world's coasts. However, we have not explored the fact that our predictors themselves and the response are prone to uncertainties. That our results are robust against the choice of prior distributions (and thus different degrees of uncertainty assigned to each parameter) suggests that our inferences are not strongly affected by these uncertainties.

Notwithstanding, there are additional uncertainties that cannot be quantified to date. For example, the onset of canyon incision has rarely been dated but can date back to several million years with repeated episodes of erosion and infilling (Maier et al., 2018; Mauffrey et al., 2017) and we have no global constraint on the age of canyon-head incision. Moreover, our predictors largely represent modern conditions, some of which may not represent active phases of canyon-head incision (e.g., Q_s , rainfall, groundwater discharge, and wave height). Other variables, such as bedload, are difficult to determine, in particular on longer timescales (e.g., Nitsche et al., 2011). Additionally, canyons may incise along tectonic faults, reoccupy fluvial valleys on the shelf (Maier et al., 2018; Mauffrey et al., 2017), or preferentially incise along shelves built by erodible stratigraphy.

Moreover, longshore sediment supply can be crucial to canyon activity (e.g., Paull et al., 2013). While we included (water) depth of closure in the analysis, the width (and transport capacity) of the ocean-littoral cell is more appropriate to characterize longshore transport. This requires the combination of closure depth with

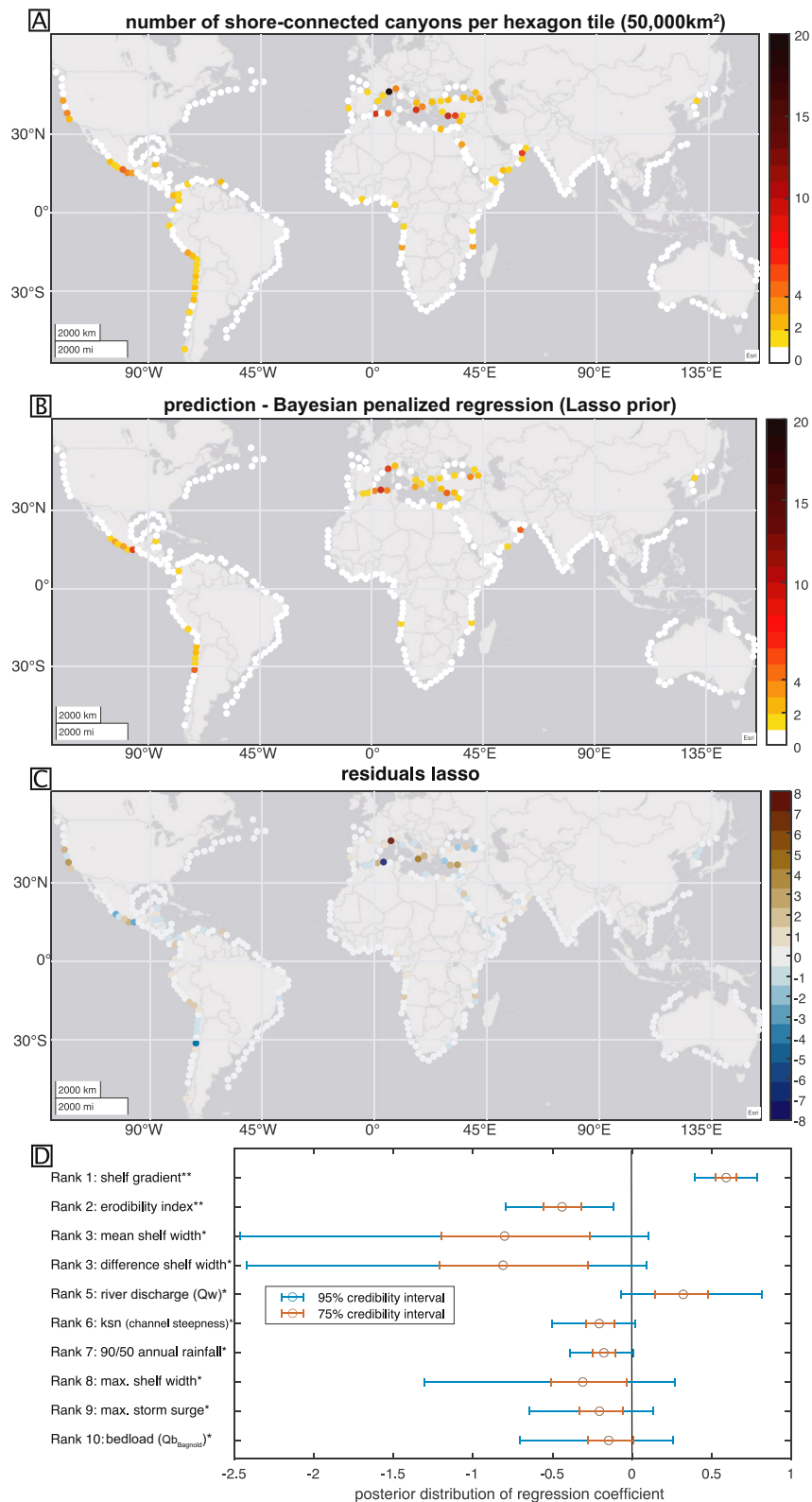


Figure 3. (a) Global map showing numbers of shore-connected canyons per hexagon, (b) prediction of shore-connected canyons numbers using Bayesian lasso-penalized regression, (c) model residuals, and (d) 95% (75%) credibility intervals of the posterior samples of the regression coefficients and ranking of the 10 most important predictors. The first (second) asterisk is shown when the 75% (95%) credible interval for the corresponding predictor does not include zero.

high-resolution coastal bathymetry, data that is still unavailable globally (Bergsma et al., 2019). Sediment supply by glacial meltwater (Normandeau & Campbell, 2020) is also not included as we focus on latitudes 50°N–50°S.

Headward canyon erosion may be enhanced by wave-driven scouring which is determined by the orientation of wave crests with regard to the canyon (Smith et al., 2018). We included fresh SGD as a predictor, however, canyon formation may also be related to seepage of recirculated seawater (Pratson et al., 2007). Additionally, erosive sediment-gravity currents can be triggered by the seasonal downward flow of dense shelfwater (Canals et al., 2006), fostering shoreward canyon-head migration. Again, the above predictors were not included as they are unavailable for the spatial scale and extent of this study.

Finally, our analysis assumes that canyons are distributed independently from each other. However, canyon presence can influence fluid escape and thus the hydrology of the neighboring canyon (Orange et al., 1994). Such coupling mechanisms induce spatial autocorrelation (e.g., clustering) in canyon occurrence which ultimately may bias our modelling results. However, our Bayesian approach embraces the idea that uncertainties about model parameters depend on data availability and our posterior distributions can be updated once new data becomes available.

4.2. Controls on Shore-Connected Canyon Occurrence

Our findings support our first hypothesis that submarine canyons preferentially remain connected to the shoreline if shelves are steep and narrow (Figures 2b and 3d). Clearly, this situation minimizes the distance that a canyon head has to erode towards the shore over a single sea-level cycle. These findings, however, contrast those of Smith et al. (2017) along the US west coast where shelf width and gradient have no predictive power on canyon occurrence, a circumstance that is likely attributed to the low variability of shelf width (~0 to <50 km) along this coast as compared to the global scale (~0–493 km).

Shoreward canyon incision during sea-level rise occurs by mass wasting or erosive sediment-gravity flows. Steep shelves promote shoreward migration of canyon heads by accelerating flow velocities and bottom-shear stresses (e.g., Middleton, 1966), and hence, increased rates of canyon-floor downcutting. Downcutting, in turn, oversteepens canyon walls resulting in mass wasting and upslope-prograding failures (Densmore et al., 1997; Pratson and Coakley, 1996) or of canyon-thalweg knickpoints supporting shoreward canyon-head erosion (Guiastrennec-Faugas et al., 2020). Shelf-sediment failure in the canyon head can initiate turbidity currents, which further erode the canyon head (Pratson and Coakley, 1996). However, continental slope gradient has no credible influence on shore-connected canyon occurrence, suggesting a minor, if any, importance of retrogressive failure along steep continental slopes as a process in shore-connection maintenance.

Our global analysis partly supports the hypothesis of Smith et al. (2018) that shore-connected canyons occur preferentially offshore tectonically active regions underlain by resistant bedrock. Indeed, the three shore-connected canyon hotspots are located along tectonically active margins. However, topographic predictors indicating high onshore relief (catchment elevation and gradient) and uplift (channel steepness [ksn]) are ranked low in our model (Table S1) or even suggest a negative relationship (Figure 3d). Such relation is counterintuitive but may be explained by the effect of vast low-relief alluvial plains (especially in large catchments) that often separate tectonically active regions from the shore on the geomorphometric variables. The erodibility index holds rank 2 and only two shore-connected canyons occur at erodibility indices >2 (Figures 2b and S2a), which supports the hypothesis that resistant lithologies are important drivers on the incision of canyon heads. In fact, that shore-connected canyons are linked to catchments with high water discharge (rank 5) and availability of river bedload (ranks 10 and 11), suggests that river bedload may promote incision into the underlying shelf stratigraphy (Cook et al., 2013; Smith et al., 2017).

Our model underestimates the occurrence of shore-connected canyons along the Californian coast and misses some of the most prominent sediment conduits along passive margins (e.g., Congo and Capbreton canyons). While the detailed reasons for underestimation remain elusive, the misfit between model and observation along the Californian margin highlights the potential role of longshore sediment transport within littoral cells, an important process documented for several Californian canyons (Covault et al., 2011; Paull

et al., 2005, 2013; Romans et al., 2009), but which we cannot include in our predictors. The singular occurrence of canyons such as the Congo also remains unclear and we can only speculate that these features occur due to conditions that could not be considered in our global assessment, such as the reoccupation of shelf-incised fluvial channels and/or underlying faults.

5. Conclusions

Canyon heads close to the 120m-depth contour, the shoreline during the LCM, are globally abundant ($n = 798$, along major continents [islands excluded] between 50°N and 50°S). Yet, presently, there are only 183 shore-connected canyons, most of which belong to three spatial hotspots: the Mediterranean active margin and the Pacific coasts of central South and Central America. Whereas non-shore-connected canyons can host active turbidity currents (Kudrass et al., 1998; Zhong & Peng, 2021), the efficiency of land-to-ocean material transfer and burial should be higher for shore-connected canyons. For example, Mediterranean shore-connected canyons efficiently transport litter and contaminants onto the basin floor (Dominguez-Carrió et al., 2020; Pierdomenico et al., 2019). Hence, we expect major terrestrially derived litter concentrations and organic carbon burial on the ocean floor where spatial hotspots of shore-connected canyons coincide with litter-producing urban areas and/or areas with high primary production and erosion rates (Hilton & West, 2020).

Using Bayesian penalized regression, we predict the spatial patterns of these hotspots using a subset of predictors. We show that shore-connected canyons prevail along margins where shelves are narrow and steep and the onshore catchments expose resistant bedrock. Hence, on a global scale, low shelf width and high shelf gradients precondition the maintenance of canyon-head connectivity to the shore as the distance a canyon head has to erode shoreward during sea-level rise is minimal and high shelf gradients foster erosive sediment-gravity flows. Our analysis confirms previous studies (Smith et al., 2017, 2018) which underscore the role of resistant bedrock exposed in onshore catchments in promoting submarine canyon incision. Together with high water discharge, these catchments deliver coarse-grained bedload which acts as a tool to erode the canyon head and floor.

Data Availability Statement

Canyon and predictor data are available in the SI and from Bernhardt and Schwanghart (2021), <https://doi.org/10.5880/figeo.2021.008>.

Acknowledgments

The authors thank Albert Kettner and Jaia Syvitski for providing Qs; Erwin Bergsma for closure depths and wave data; Elco Luijendijk for SGDs and Nils Moosdorf for erodibility indices. Reviews from Michael Clare and one anonymous reviewer greatly improved the manuscript.

References

- Azaroff, A., Miossec, C., Lancelot, L., Guyoneaud, R., & Monperrus, M. (2020). Priority and emerging micropollutants distribution from coastal to continental slope sediments: A case study of Capbreton Submarine Canyon (North Atlantic Ocean). *The Science of the Total Environment*, 703, 135057. <https://doi.org/10.1016/j.scitotenv.2019.135057>
- Bagnold, R. A. (1966). *An approach to the sediment transport problem from general physics*. U.S. Geol. Surv. Prof. Paper 422-I.37.
- Becker, J. J., Sandwell, D. T., Smith, W. H. F., Braud, J., Binder, B., Depner, J., et al. (2009). Global bathymetry and elevation data at 30 arc seconds resolution: SRTM30_PLUS. *Marine Geodesy*, 32, 355–371. <https://doi.org/10.1080/01490410903297766>
- Bergsma, E. W. J., & Almar, R. (2020). Coastal coverage of ESA Sentinel 2 mission. *Advances in Space Research*, 65, 2636–2644. <https://doi.org/10.1016/j.asr.2020.03.001>
- Bergsma, E. W. J., Almar, R., & Maisongrande, P. (2019). Radon-augmented Sentinel-2 satellite imagery to derive wave-patterns and regional bathymetry. *Remote Sensing*, 11, 1918–2016. <https://doi.org/10.3390/rs11161918>
- Bernhardt, A., & Schwanghart, W. (2021). *Global dataset of submarine canyon heads combined with terrestrial and marine topographic and oceanographic parameters*. GFZ Data Services. <https://doi.org/10.5880/figeo.2021.008>
- Boers, N., Bookhagen, B., Barbosa, H. M. J., Marwan, N., Kurths, J., & Marengo, J. A. (2014). Prediction of extreme floods in the eastern Central Andes based on a complex networks approach. *Nature Communications*, 5, 1–7. <https://doi.org/10.1038/ncomms6199>
- Canals, M., Puig, P., de Madron, X. D., Heussner, S., Palanques, A., & Fabres, J. (2006). Flushing submarine canyons. *Nature*, 444, 354–357. <https://doi.org/10.1038/nature05271>
- Cook, K. L., Turowski, J. M., & Hovius, N. (2013). A demonstration of the importance of bedload transport for fluvial bedrock erosion and knickpoint propagation. *Earth Surface Processes and Landforms*, 38, 683–695. <https://doi.org/10.1002/esp.3313>
- Covault, J. A., Normark, W. R., Romans, B. W., & Graham, S. A. (2007). Highstand fans in the California borderland: The overlooked deep-water depositional systems. *Geology*, 35, 783–786. <https://doi.org/10.1130/g23800a.1>
- Covault, J. A., Romans, B. W., Graham, S. A., Fildani, A., & Hillel, G. E. (2011). Terrestrial source to deep-sea sink sediment budgets at high and low sea levels: Insights from tectonically active Southern California. *Geology*, 39, 619–622. <https://doi.org/10.1130/g31801.1>
- Densmore, A. L., Anderson, R. S., McAdoo, B. G., & Ellis, M. A. (1997). Hillslope evolution by bedrock landslides. *Science*, 275(80), 369–372. <https://doi.org/10.1126/science.275.5298.369>

- Dominguez-Carri6, C., Sanchez-Vidal, A., Estournel, C., Corbera, G., Riera, J. L., Orejas, C., et al. (2020). Seafloor litter sorting in different domains of Cap de Creus continental shelf and submarine canyon (NW Mediterranean Sea). *Marine Pollution Bulletin*, 161, 111744. <https://doi.org/10.1016/j.marpolbul.2020.111744>
- Efron, B. (2013). Bayes' theorem in the 21st century. *Science*, 340(80), 1223–1226. <https://doi.org/10.1126/science.1236536>
- Fekete, B. M., V6r6smarty, C. J., Grabs, W., 2002. High-resolution fields of global runoff combining observed river discharge and simulated water balances. *Global Biogeochemical Cycles* 16, 15–1. <https://doi.org/10.1029/1999gb001254>
- Galy, V., France-Lanord, C., Beyssac, O., Faure, P., Kudrass, H., & Palhol, F. (2007). Efficient organic carbon burial in the Bengal fan sustained by the Himalayan erosional system. *Nature*, 450, 407–410. <https://doi.org/10.1038/nature06273>
- Guiastrennec-Faugas, L., Gillet, H., Silva Jacinto, R., Dennielou, B., Hanquiez, V., Schmidt, S., et al. (2020). Upstream migrating knick-points and related sedimentary processes in a submarine canyon from a rare 20-year morphobathymetric time-lapse (Capbreton submarine canyon, Bay of Biscay, France). *Marine Geology*, 423, 106143. <https://doi.org/10.1016/j.margeo.2020.106143>
- Hage, S., Cartigny, M. J. B., Sumner, E. J., Clare, M. A., John, E., Clarke, H., et al. (2019). Direct monitoring reveals initiation of turbidity currents from extremely dilute river plumes. *Geophysical Research Letters*, 46(20), 11310–11320. <https://doi.org/10.1029/2019GL084526>
- Hallermeier, R. J. (1980). A profile zonation for seasonal sand beaches from wave climate. *Coastal Engineering*, 4, 253–277. [https://doi.org/10.1016/0378-3839\(80\)90022-8](https://doi.org/10.1016/0378-3839(80)90022-8)
- Harris, P. T., Macmillan-lawler, M., Rupp, J., & Baker, E. K. (2014). Geomorphology of the oceans. *Marine Geology*, 352, 4–24. <https://doi.org/10.1016/j.margeo.2014.01.011>
- Harris, P. T., & Whiteway, T. (2011). Global distribution of large submarine canyons: Geomorphic differences between active and passive continental margins. *Marine Geology*, 285, 69–86. <https://doi.org/10.1016/j.margeo.2011.05.008>
- Hilton, R. G., & West, A. J. (2020). Mountains, erosion and the carbon cycle. *Nature Reviews Earth & Environment*, 1, 284–299. <https://doi.org/10.1038/s43017-020-0058-6>
- Kane, I. A., & Clare, M. A. (2019). Dispersion, accumulation, and the ultimate fate of microplastics in deep-marine environments: A review and future directions. *Frontiers of Earth Science*, 7. <https://doi.org/10.3389/feart.2019.00080>
- Korup, O. (2021). Bayesian geomorphology. *Earth Surface Processes and Landforms*, 46, 151–172. <https://doi.org/10.1002/esp.4995>
- Kudrass, H. R., Michels, K. H., Wiedicke, M., & Suckow, A. (1998). Cyclones and tides as feeders of a submarine canyon off Bangladesh. *Geology*, 26(8), 715–718. [https://doi.org/10.1130/0091-7613\(1998\)02610.1130/0091-7613\(1998\)026<0715:catafo>2.3.co;2](https://doi.org/10.1130/0091-7613(1998)02610.1130/0091-7613(1998)026<0715:catafo>2.3.co;2)
- Lehner, B., Verdin, K., & Jarvis, A. (2008). New global hydrography derived from spaceborne elevation data. *Eos, Transactions American Geophysical Union*, 89, 93–94. <https://doi.org/10.1029/2008eo100001>
- Li, Y., Clift, P. D., B6ning, P., Blusztajn, J., Murray, R. W., Ireland, T., et al. (2018). Continuous Holocene input of river sediment to the Indus Submarine Canyon. *Marine Geology*, 406, 159–176. <https://doi.org/10.1016/j.margeo.2018.09.011>
- Luijendijk, E., Gleeson, T., & Moosdorf, N. (2020). Fresh groundwater discharge insignificant for the world's oceans but important for coastal ecosystems. *Nature Communications*, 11, 1260. <https://doi.org/10.1038/s41467-020-15064-8>
- Maier, K. L., Johnson, S. Y., & Hart, P. (2018). Controls on submarine canyon head evolution: Monterey Canyon, offshore central California. *Marine Geology*, 404, 24–40. <https://doi.org/10.1016/j.margeo.2018.06.014>
- Makalic, E., & Schmidt, D. F. (2011). A simple Bayesian algorithm for feature ranking in high dimensional regression problems. *Lecture notes in computer science (including subseries lecture notes in artificial intelligence and lecture notes in bioinformatics)* 7106 LNAI, 223–230. https://doi.org/10.1007/978-3-642-25832-9_23
- Makalic, E., & Schmidt, D. F. (2016). *High-dimensional Bayesian regularised regression with the BayesReg package* (pp. 1–18). arXiv:1611.06649
- Mauffrey, M.-A., Urgeles, R., Bern6, S., & Canning, J. (2017). Development of submarine canyons after the Mid-Pleistocene Transition on the Ebro margin, NW Mediterranean: The role of fluvial connections. *Quaternary Science Reviews*, 158, 77–93. <https://doi.org/10.1016/j.quascirev.2017.01.006>
- M6tivier, F., Meunier, P., Moreira, M., Crave, A., Chaduteau, C., Ye, B., & Liu, G. (2004). *Transport dynamics and morphology of a high mountain stream during the peak flow season: The 6rimqi River (Chinese Tian Shan)* (pp. 769–776). River Flow. <https://doi.org/10.1201/b16998-99>
- Meunier, P., M6tivier, F., Lajeunesse, E., M6riaux, A.S., & Faure, J. (2006). Flow pattern and sediment transport in a braided river: The “torrent de St Pierre” (French Alps). *Journal of Hydrology*, 330, 496–505. <https://doi.org/10.1016/j.jhydrol.2006.04.009>
- Middleton, G. V. (1966). Experiments on density and turbidity currents: II. Uniform flow of density currents. *Canadian Journal of Earth Sciences*, 3, 627–637. <https://doi.org/10.1139/e66-044>
- Moosdorf, N., Cohen, S., & von Hagke, C. (2018). A global erodibility index to represent sediment production potential of different rock types. *Applied Geography*, 101, 36–44. <https://doi.org/10.1016/j.apgeog.2018.10.010>
- Mountjoy, J. J., Howarth, J. D., Orpin, A. R., Barnes, P. M., Bowden, D. A., Rowden, A. A., et al. (2018). Earthquakes drive large-scale submarine canyon development and sediment supply to deep-ocean basins. *Science Advances*, 4(3), eaar3748. <https://doi.org/10.1126/sciadv.aar3748>
- Muis, S., Verlaan, M., Winsemius, H. C., Aerts, J. C. J. H., & Ward, P. J. (2016). A global reanalysis of storm surges and extreme sea levels. *Nature Communications*, 7, 11969. <https://doi.org/10.1038/ncomms11969>
- Nitsche, M., Rickenmann, D., Turowski, J. M., Badoux, A., & Kirchner, J. W. (2011). Evaluation of bedload transport predictions using flow resistance equations to account for macro-roughness in steep mountain streams. *Water Resources Research*, 47. <https://doi.org/10.1029/2011wr010645>
- Normandeau, A., & Campbell, D. C. (2020). Recurrence of turbidity currents on glaciated continental margins: A conceptual model from Eastern Canada. *Journal of Sedimentary Research*, 90, 1305–1321. <https://doi.org/10.2110/jsr.2020.66>
- Normark, W. R., Normark, W., Piper, D., Piper, D., Covault, J. A., Romans, B., et al. (2009). Submarine canyon and fan systems of the California Continental Borderland. *Earth Science in the Urban Ocean: The Southern California Continental Borderland*, 454, 141–168. [https://doi.org/10.1130/2009.2454\(2.7\)](https://doi.org/10.1130/2009.2454(2.7))
- Orange, D. L., Anderson, R. S., & Breen, N. A. (1994). Regular canyon spacing in the submarine environment the link between hydrology and geomorphology. *Geological Society of America Today*. 4(2), 35–39. Retrieved from <https://www.geosociety.org/gsatoday/archive/4/2/pdf/i1052-5173-4-2-sci.pdf>
- Paull, C. K., Caress, D. W., Lundsten, E., Gwiazda, R., Anderson, K., McGann, M., et al. (2013). Anatomy of the La Jolla Submarine Canyon system; Offshore southern California. *Marine Geology*, 335, 16–34. <https://doi.org/10.1016/j.margeo.2012.10.003>
- Paull, C. K., Mitts, P., Ussler, W., Keaten, R., & Greene, H. G. (2005). Trail of sand in upper Monterey Canyon: Offshore California. *Geological Society of America Bulletin*, 117, 1134–1145. <https://doi.org/10.1130/b25390.1>
- Pierdomenico, M., Casalbone, D., & Chiocci, F. L. (2019). Massive benthic litter funnelled to deep sea by flash-flood generated hyperpycnal flows. *Scientific Reports*, 9, 1–10. <https://doi.org/10.1038/s41598-019-41816-8>

- Pratson, L. F., & Coakley, B. J. (1996). A model for the headward erosion of submarine canyons induced by downslope-eroding sediment flows. *Geological Society of America Bulletin*, 108, 225–234. [https://doi.org/10.1130/0016-7606\(1996\)108<0225:amfthe>2.3.co;2](https://doi.org/10.1130/0016-7606(1996)108<0225:amfthe>2.3.co;2)
- Pratson, L. F., Nittrouer, C. A., Wiberg, P. L., Steckler, M. S., Swenson, J. B., Cacchione, D. A., et al. (2007). Seascape evolution on clastic continental shelves and slopes. *Continental margin sedimentation* (pp. 339–380). <https://doi.org/10.1002/9781444304398.ch7>
- Pratson, L. F., Ryan, W. B. F., Mountain, G. S., & Twichell, D. C. (1994). Submarine canyon initiation by downslope-eroding sediment flows: Evidence in late Cenozoic strata on the New Jersey continental slope. *GSA Bulletin*, 106(3), 395–412. [https://doi.org/10.1130/0016-7606\(1994\)106<0395:SCIBDE>2.3.CO;2](https://doi.org/10.1130/0016-7606(1994)106<0395:SCIBDE>2.3.CO;2)
- Rogers, K. G., Goodbred, S. L., & Khan, S. R. (2015). Shelf-to-canyon connections: Transport-related morphology and mass balance at the shallow-headed, rapidly aggrading Swatch of No Ground (Bay of Bengal). *Marine Geology*, 369, 288–299. <https://doi.org/10.1016/j.margeo.2015.09.011>
- Romans, B. W., Normark, W. R., McGann, M. M., Covault, J. A., & Graham, S. A. (2009). Coarse-grained sediment delivery and distribution in the Holocene Santa Monica Basin, California: Implications for evaluating source-to-sink flux at millennial time scales. *Geological Society of America Bulletin*, 121, 1394–1408. <https://doi.org/10.1130/b26393.1>
- Schwanghart, W., & Scherler, D. (2014). Short Communication: TopoToolbox 2 – MATLAB-based software for topographic analysis and modeling in Earth surface sciences. *Earth Surface Dynamics*, 2, 1–7. <https://doi.org/10.5194/esurf-2-1-2014>
- Shedlock, K., Giardini, D., Gruenthal, G., & Zhang, P. (2000). The GSHAP global seismic hazard map. *Seismological Research Letters*, 71, 679–686. <https://doi.org/10.1785/gssrl.71.6.679>
- Shepard, F. P. (1981). Submarine canyons: Multiple causes and long-time persistence. *American Association of Petroleum Geologists Bulletin*, 65, 1062–1077.
- Smith, M. E., Finnegan, N. J., Mueller, E. R., Best, R. J., 2017. Durable terrestrial bedrock predicts submarine canyon formation. *Geophysical Research Letters* 44, 10332–10340. <https://doi.org/10.1002/2017gl075139>
- Smith, M. E., Werner, S. H., Buscombe, D., Finnegan, N. J., Sumner, E. J., Mueller, E. R., 2018. Seeking the shore: Evidence for active submarine canyon head incision due to coarse sediment supply and focusing of wave energy. *Geophysical Research Letters* 45(22), 12403–12413. <https://doi.org/10.1029/2018gl080396>
- Stolle, A., Schwanghart, W., Andermann, C., Bernhardt, A., Fort, M., Jansen, J. D., et al. (2019). Protracted river response to medieval earthquakes. *Earth Surface Processes and Landforms*, 44, 331–341. <https://doi.org/10.1002/esp.4517>
- Sweet, M. L., & Blum, M. D. (2016). Connections between fluvial to shallow marine environments and submarine canyons: Implications for sediment transfer to deep water. *Journal of Sedimentary Research*, 86, 1147–1162. <https://doi.org/10.2110/jsr.2016.64>
- Syvitski, J. P. M., & Kettner, A. (2011). Sediment flux and the anthropocene. *Philosophical Transactions of the Royal Society A: Mathematical, Physical and Engineering Sciences*, 369, 957–975. <https://doi.org/10.1098/rsta.2010.0329>
- Syvitski, J. P. M., & Saito, Y. (2007). Morphodynamics of deltas under the influence of humans. *Global and Planetary Change*, 57(3–4), 261–282. <https://doi.org/10.1016/j.gloplacha.2006.12.001>
- Tibshirani, R. (2011). Regression shrinkage and selection via the lasso: A retrospective. *Journal of the Royal Statistical Society Series B (Statistical Methodology)*, 73, 273–282. <https://doi.org/10.1111/j.1467-9868.2011.00771.x>
- van Erp, S. (2020). A tutorial on Bayesian penalized regression with shrinkage priors for small sample sizes. In R. van de Schoot, & M. Miočević (Eds.), *Small sample size solutions* (pp. 71–84). Routledge. <https://doi.org/10.4324/9780429273872-6>
- van Erp, S., Oberski, D. L., & Mulder, J. (2019). Shrinkage priors for Bayesian penalized regression. *Journal of Mathematical Psychology*, 89, 31–50. <https://doi.org/10.1016/j.jmp.2018.12.004>
- Zhong, G., & Peng, X. (2021). Transport and accumulation of plastic litter in submarine canyons—The role of gravity flows. *Geology*, 49(5), 581–586. <https://doi.org/10.1130/G48536.1>

References From the Supporting Information

- Baddeley, A., Rubak, E., & Turner, R. (2015). *Spatial point patterns: Methodology and applications with R*. Apple Academic Press Inc. <https://doi.org/10.1201/b19708>
- Gelman, A., Hwang, J., & Vehtari, A. (2013). Understanding predictive information criteria for Bayesian models. *Statistics and Computing*, 24, 997–1016. <https://doi.org/10.1007/s11222-013-9416-2>
- Watanabe, S. (2010). Asymptotic equivalence of Bayes cross validation and widely applicable information criterion in singular learning theory. *Journal of Machine Learning Research*, 11, 3571–3594.